Available Online

J. Sci. Res. **14** (1), 229-242 (2022)

JOURNAL OF SCIENTIFIC RESEARCH

www.banglajol.info/index.php/JSR

Mechanical, Elastic and Thermal Properties of Hexagonal BC_2N Superhard Material

N. Chaurasiya[1, 2*], S. Rai[1], P. K. Yadawa[1]

[1]Department of Physics, Prof. Rajendra Singh (Rajju Bhaiya) Institute of Physical Sciences for Study and Research, V. B. S. Purvanchal University, Jaunpur, India-222003

[2]Department of Mechanical Engineering, UNSIET, V. B. S. Purvanchal University, Jaunpur, India-222003

Received 5 August 2021, accepted in final revised form 22 September 2021

Abstract

The ultrasonic properties of the hexagonal BC_2N superhard material were studied at temperature-dependent following the interaction potential model. Higher-order elastic constants are used for the determination of other ultrasonic parameters. The temperature variation of the ultrasonic velocities is evaluated along with different angles with z-axis (unique axis) of the crystal using the second-order elastic constants temperature variation of the thermal relaxation time, and Debye average velocities are also calculated along with the same orientation. The temperature dependency of the acoustic properties is discussed in correlation with elastic, thermal, and mechanical properties. It has been found that thermal conductivity and thermal energy density are the main contributors to the behavior of ultrasonic attenuation as a function of temperature. The responsible cause of attenuation is phonon-phonon interaction. Mechanical properties of BC_2N superhard material at temperature 400K are better than at other temperatures because, at this temperature, it has low ultrasonic attenuation. Superhard material BC_2N has many industrial and engineering applications.

Keywords: Superhard material; Thermal conductivity; Elastic properties; Ultrasonic properties.

doi: http://dx.doi.org/10.3329/jsr.v14i1.55038 J. Sci. Res. **14** (1), 229-242 (2022)

1. Introduction

Over the past few decades, B-C-N compounds were attracted important attention due to their predictable intermediates [1-3] or better properties than carbon and boron nitrides [4-6]. Super materials can provide special performance in a wide variety of applications. In particular, a covalent insulator with simple electronic and lattice structures for Diamond has long been known as one of the hardest [7] and highest thermometer conductive materials [8,9]. Consequently, discovering superhard thermometer conductive materials with desirable properties is a recurring subject in condensed matter physics and materials science. BC_2N has attracted widespread attention because it is expected to be thermally

* *Corresponding author*: naveenchaurasia90@gmail.com

and chemically more stable than diamond and harder than C-BN [10,11]. BC_2N has gained much attention due to its high Stiffness and improved stability in structure, and many studies have intensive on it [12,13]. The BC_2N has gained much attention due to its high Vickers hardness (up to 76 G Pa) and good stability and ductility [14,15]. It includes a superposition of collapsed layers of honeycomb C and hexagonal B-N. In addition, the B or N atoms project into the B-N layer at the center of the carbon hexagonal rings. Recently, Chakraborty *et al*. [16] exposed that hexagonal diamond and wurtzite boron nitride are two superhard materials compared to their cubic diamond, cubic counterparts, and cubic boron nitride.

Superhard materials have become a unique resource in modern industry, benefiting from the high hardness beyond ordinary materials. For example, cutting and polishing equipment widely used in manufacturing [17-19], ultra-rigid drill bits that are commonly used in exploration [20], and semiconductor equipment working in extreme environments [21,22] of superhard material are inseparable from the application. Over the past few decades, B-C-N compounds have attracted significant interest due to their expected intermediates or better properties than carbon and boron nitrides [23,24].

A single-phase hexagonal close-packed structure in the BC_2N system has been successfully fabricated by arc melting. Structure analysis of the annealed (homogenized) samples reveals that the HCP phase is thermally stable. Ultrasonic attenuation (UA) is a very important physical parameter to characterize the material, which is well related to several physical quantities like thermal conductivity, specific heat, thermal energy density, and second and third-order elastic constants (SOECs & TOECs). The elastic constants provide valuable information about the structural stability of the superhard material [25].

In our present evaluation, we predict the ultrasonic properties of hexagonal structured BC_2N superhard material at different temperatures. BC_2N superhard material will improve the mechanical properties of other simple structure materials and their performance and play a significant role in the manufacturing apparatus with useful physical properties under moderate working conditions. For that, we have considered ultrasonic attenuation coefficient, acoustic coupling constants, elastic Stiffness constant, thermal relaxation time, and the ultrasonic velocity for BC_2N superhard compound. Bulk modulus (B), shear modulus (G), Young's modulus (Y), Pugh's ratio (B/G), and Poisson's ratio were also calculated and discussed for superhard materials.

2. Theory

There are numerous methods to analyses high-order (SOECs, TOECs) elastic factors of hexagonal materials. Meanwhile, a first-principal technique based on density functional theory (DFT) within the quasi-harmonic approximation (QHA) and generalized gradient approximation (GGA) is commonly used for the determination of second and third-order elastic constants. The interaction potential model technique is similarly one of the furthermost well-established principles for calculating high-order (SOECs and TOECs)

elastic constants of hexagonally structured material. The present work used the Lenard Jones interaction potential model approach to evaluate second and third-order elastic constants.

A comprehensive description of n^{th} order elastic constant is the partial results of the thermodynamic potential of the average constrained to finite deformation as well as mathematically conveyed by subsequent expression as [26,27]

$$C_{ijklmn\ldots} = \frac{\partial^n F}{\partial\eta_{ij}\partial\eta_{kl}\partial\eta_{mn\ldots.}} \tag{1}$$

Whenever F is denoted free energy density and η_{ij} is denote Lagrangian strain component tensor. F may be extended in relations to strain η by Taylor series expansion as:

$$F = \sum_{n=0}^{\infty} F_n = \sum_{n=0}^{\infty} \frac{1}{n!}\left(\frac{\partial^n F}{\partial\eta_{ij}\partial\eta_{kl}\partial\eta_{mn\ldots}}\right)\eta_{ij}\eta_{kl}\eta_{mn}\ldots \tag{2}$$

Thereby, the free energy density is written such as:

$$F_2 + F_3 = \frac{1}{2!}C_{ijkl}\eta_{ij}\eta_{kl} + \frac{1}{3!}C_{ijklmn}\eta_{ij}\eta_{kl}\eta_{\mathrm{mn}} \tag{3}$$

In order that HCP compounds, the basis vectors are $a_1 = a\left(\frac{\sqrt{3}}{2}, \frac{1}{2}, 0\right)$, $a_2 = a(0,1,0)$ and $a_3 = a(0,0,c)$ in cartesian coordinates axes. Where a and c represent the unit cell lattice parameters. The unit cell of hexagonal compound contains two nonequivalent atoms: 6- atoms in basal plane and 3-3 atoms upper and lower the basal plane. The consequently, both first and second neighborhood contains six atoms. Were $r_1 = a(0,0,0)$ and $r_2 = \left(\frac{a}{2\sqrt{3}}, \frac{a}{2}, \frac{c}{2}\right)$ are the position vectors. The energy density is examined to be function of Lennard Jones potential and specified as:

$$\varphi(r) = -\frac{a_0}{r^m} + \frac{b_0}{r^n} \tag{4}$$

Where a_0, b_0 are coefficients constants; m, n represents the integers, and r is the distance between atoms. Establish the interaction potential model leads to computed six SOECs and ten TOECs of the hexagonal compound, and formulations of elastic constants are given as following expressions [26,27]

$$\left.\begin{array}{ll} C_{11} = 24.1\ \mathrm{p}^4C' & C_{12} = 5.918\ \mathrm{p}^4C' \\ C_{13} = 1.925\ \mathrm{p}^6C' & C_{33} = 3.464\ \mathrm{p}^8C' \\ C_{44} = 2.309p^4C' & C_{66} = 9.851\ \mathrm{p}^4C' \end{array}\right\} \tag{5a}$$

$$\left.\begin{array}{ll} C_{111} = 126.9p^2B + 8.853p^4C' & C_{112} = 19.168p^2B - 1.61p^4C' \\ C_{113} = 1.924p^4B + 1.155p^6C' & C_{123} = 1.617p^4B - 1.155p^6C' \\ C_{133} = 3.695p^6B & C_{155} = 1.539p^4B \\ C_{144} = 2.309p^4B & C_{344} = 3.464p^6B \\ C_{222} = 101.039p^2B + 9.007p^4C' & C_{333} = 5.196p^8B \end{array}\right\} \tag{5b}$$

where p = c/a: axial ratio;$C' = \chi$ a / p^5; $B = \psi\ \mathrm{a}^3/p^3$; $\chi = (1/8)[\{nb_0\ (n-m)\}/\{\ \mathrm{a}^{n+4}\}]$ $\psi = -\chi$ /{6 $\mathrm{a}^2(m+n+6)$}; m, n=integer quantity; b_0=Lennard- Jones parameter

The bulk and shear modulus were calculated using Voigt and Reuss' methodologies [28,29]. Correspondingly, the calculations of unvarying stress and unvarying strain were used in Voigt and Reuss' methodologies. Furthermore, From Hill's methods, the average values of both methodologies were used toward ensuing computing values of B and G [30]. Young's modulus and Poisson's ratio are considered using values of bulk modulus and shear modulus, respectively [31-34]. The following expressions were used for the evaluation of Y, B, G, and σ.

$$\left.\begin{array}{ll} M = C_{11} + C_{12} + 2C_{33} - 4C_{13}; & \mathrm{C}^2 = (C_{11} + C_{12})C_{33} - 4C_{13} + C^2{}_{13}; \\ B_R = \frac{C^2}{M}; & \mathrm{B}_V = \frac{2(C_{11}+C_{12})+4C_{13}+C_{33}}{9}; \\ G_V = \frac{M+12(C_{44}+C_{66})}{30}; & \mathrm{G}_R = \frac{5C^2C_{44}C_{66}}{2[3B_VC_{44}C_{66}+C^2(C_{44}+C_{66})]}; \\ Y = \frac{9GB}{G+3B}; \quad \mathrm{B} = \frac{B_V+B_R}{2}; & \mathrm{G} = \frac{G_V+G_R}{2}; \quad \sigma = \frac{\mathrm{3B\text{-}2G}}{2(\mathrm{3B}+G)} \end{array}\right\} \quad (6)$$

The anisotropic and mechanical properties of nanostructured materials are well correlated with ultrasonic velocity due to the velocity of ultrasonic waves mainly depends upon the density and SOECs. As a function of vibration mode, those are three types of ultrasonic velocities in hexagonal nanostructured compounds. First longitudinal V_L and second shear (V_{S1}, V_{S2}) waves velocities. Ultrasonic velocities based on the angle between the direction of propagation and z-axis for the hexagonal nanostructured compound are given by a subsequent set of equations:

$$\left.\begin{array}{l} V_L^2 = \{C_{33}\,cos^2\theta + C_{11}\,sin^2\theta + C_{44} + \{[C_{11}\,sin^2\theta - C_{33}\,cos^2\theta + C_{44}(cos^2\theta - sin^2\theta)]^2 \\ +4\,cos^2\theta\,sin^2\theta\,(C_{13}+C_{44})^2\}^{1/2}\}/2\rho \\ V_{S1}^2 = \{C_{33}\,cos^2\theta + C_{11}\,sin^2\theta + C_{44} - \{[C_{11}\,sin^2\theta - C_{33}\,cos^2\theta + C_{44}(cos^2\theta - sin^2\theta)]^2 \\ +4\,cos^2\theta\,sin^2\theta\,(C_{13}+C_{44})^2\}^{1/2}\}/2\rho \\ V_{S2}^2 = \{C_{44}\,cos^2\theta + C_{66}\,sin^2\theta\}/\rho \end{array}\right\} \quad (7)$$

where, V_L, V_{S1}, and V_{S2} are the longitudinal, quasi-shear, and shear wave velocities. Also, ρ is the density of compound and θ is the angle with the unique axis of the crystal. The Debye average velocity is specified by the equation as [35,36]

$$V_D = \left[\frac{1}{3}\left(\frac{1}{V_L^3} + \frac{1}{V_{s1}^3} + \frac{1}{V_{s2}^3}\right)\right]^{-1/3} \quad (8)$$

The mathematical formulation of ultrasonic attenuation for longitudinal $(A)_{Long}$ and shear waves $(A)_{\mathrm{Shear}}$ induced by the energy loss due to electron-phonon interaction is given by:

$$A_{long} = \frac{2\pi^2 f^2}{\rho V_l^3}\left(\frac{4}{3}\eta_e + \chi\right) \quad (9)$$

$$A_{shear} = \frac{2\pi^2 f^2}{\rho V_S^3}\eta_e \quad (10)$$

where 'ρ' is the density of nanostructured compound, 'η_e' is the electron viscosity, 'f' is the frequency of the ultrasonic wave, and 'χ' is the compressional viscosity, V_L and V_S are the acoustic wave velocities for longitudinal and shear waves respectively and are given as:

$$V_L = \sqrt{\frac{C_{33}}{\rho}} \text{ and } \quad V_S = \sqrt{\frac{C_{44}}{\rho}}$$

The viscosity of the electron gas (η_e) [35,36] is given by

$$\eta_e = \frac{9\times10^{11}\hbar^2\left(3\pi^2 N\right)^{2/3}}{5e^2 R} \tag{11}$$

Wherever '*N*' represents the number of molecules per unit volume, and '*R*' is the resistivity.

For p-p interaction (Akhieser's type loss) (at high temperature) and thermoelastic loss are the two prevailing processes, whichever are considerable for attenuation of ultrasonic wave. The attenuation by virtue of Akhieser's loss is specified by the subsequent equation:

$$(A/f^2)_{Akh} = \frac{4\pi^2\tau E_0 (D/3)}{2\rho V^3} \tag{12}$$

Here, f represents the frequency of the ultrasonic wave; E_0 is the thermal energy density. The measure of transforming acoustical energy into thermal energy is recognized as acoustical coupling constants, signified by *D*, and is specified by the subsequent expression:

$$D = 3(3E_0 < (\gamma_i^j)^2 > - < \gamma_i^j >^2 C_V T)/E_0 \tag{13}$$

where C_V is the specific heat per unit volume of the material, *T* is the temperature and γ_i^j is the Grüneisen number. While the ultrasonic waves are transmitted through the material, the equilibrium of lattice phonon distribution gets disturbed. The time takes for re-establishment of equilibrium of the thermal phonons is named as thermal relaxation time, signified by τ, and is specified by the subsequent expression:

$$\tau = \tau_S = \tau_L/2 = \frac{3k}{C_V V_D^2} \tag{14}$$

Wherever τ_L and τ_S are the thermal relaxation time for the longitudinal wave and shear, 'k' is the thermal conductivity of the nanostructured compound.

The thermoelastic loss $(A/f^2)_{Th}$ is considered by the following equation [35,36]:

$$(A/f^2)_{Th} = 4\pi^2 < \gamma_i^j >^2 \frac{kT}{2\rho V_L^5} \tag{15}$$

The total ultrasonic attenuation is specified by the subsequent equation as:

$$(A/f^2)_{Total} = (A/f^2)_{Th} + (A/f^2)_L + (A/f^2)_S \tag{16}$$

Wherever $(A/f^2)_{Th}$ is the thermoelastic loss, $(\frac{A}{f^2)_L}$and $(A/f^2)_S$ are the ultrasonic attenuation coefficient for the longitudinal wave and shear wave correspondingly.

3. Results and Discussion

3.1. *Higher-order elastic constants*

We have calculated the elastic constants (six SOECs and ten TOECs) in the current analysis using Lennard-Jones's potential model. The lattice parameters '*a*' (basal plane parameter) and '*p*' (axial ratio) for BC_2N superhard material are 2.528Å, and 4.967

respectively [37]. The value of *m* and *n* for chosen superhard material are 6 and 7. The value of b_0 is 1.695×10^{-64} erg cm^7 for BC_2N superhard material. The values of second and third-order elastic constants that were calculated for this superhard material are presented in Table 1.

Table 1. SOEC and TOEC (in GPa) of BC_2N at room temperature.

BC_2N	C_{11}	C_{12}	C_{13}	C_{33}	C_{44}	C_{66}	B
Present work	1019	250	226	1265	271	399	547
[37]	1049	113	65.18	1055	406	468	404

BC_2N	C_{111}	C_{112}	C_{113}	C_{123}	C_{133}	C_{344}	C_{144}	C_{155}	C_{222}	C_{333}
Present work	-16629	-2636	-579	-736	-3805	-3567	-857	-571	-13157	-14833

BC_2N superhard material had the highest elastic constant values, which are important for the material, as these are associated with the stiffness parameter. SOECs are used to determine the UA and associated parameters. The highest elastic constant value found for superhard materials is indicative of their better mechanical properties over other superhard materials.

Evidently, for a steady hexagonal structure compound, the five independent SOECs (Cij, namely C_{11}, C_{12}, C_{13}, C_{33}, C_{44}) would satisfy the well-known Born- Huang's stability norms [31,32] i.e., $C_{11} - |C_{12}| > 0$, $(C_{11}+C_{12})\, C_{33} - 2C^2_{13} > 0$, $C_{11} > 0$ and $C_{44} > 0$. This is understandable since Table-1. It is evident that the value of elastic constants is positive, too, satisfies the Born-Huang's mechanical stability constraints, and therefore totally these compounds are mechanically stable. Using the formula bulk modulus $B = 2(C_{11}+ C_{12}+ 2C_{13} + C_{33}/2)/9$, the B for BC_2N superhard material be calculated and presented in Table 1. The evaluated values of C_{44} and C_{66} are few different than other theoretical results for the BC_2N superhard compound. Essentially Sadeghi *et al*. [37] has been theoretically evaluated by DFT investigations, which is rather different from the present method. Although obtained order of SOEC is of the same as given in Table 1. The relative magnitude of C_{11}, C_{12} C_{13} C_{33} is well presented by our theoretical approach. Thus, there is good agreement between the presented and the reported second-order elastic constants and bulk modulus. Therefore, our theoretical approach for calculating second-order elastic constants for hexagonal structured superhard compounds at room temperature is well justified. We present the calculated values of TOECs in Table 1. The negative values of third-order elastic constants indicate a negative strain in the solid. However, third-order elastic constants are not compared due to a lack of data in the literature. However, the negative third-order elastic constants are found in previous papers for hexagonal structure materials. Therefore, the theory applied to valuation higher-order elastic constants is justified [38,39]. Hence the applied theory for the valuation of higher-order elastic constants is justified.

The values of B, G, Y, B/G, and σ for BC_2N superhard compound at room temperature are calculated using equation (1) and existing in Table 2.

Table 2. Voigt–Reuss' constants (M and $C^{2)}$, B ($\times 10^{10}$Nm^{-2}), G ($\times 10^{10}$Nm^{-2}), Y ($\times 10^{10}$Nm^{-2}), σ, B/G, for BC_2N superhard material.

	M	C^2	B_r	B_v	G_r	G_v	Y	B/G	G/B	σ
BC_2N	2895	1655457	571	523	403.47	364.5	933.66	1.43	0.70	0.22

It is found that the values of B, Y, and G are BC_2N superhard materials. Thus, BC_2N superhard materials have little Stiffness and bonding concerning transition-metal disilicides. B/G and 'σ' are the measures of brittleness and ductility of solid. If σ = 0.22≤0.26 and B/G = 1.43≤1.75, the solid is generally brittle; otherwise, it is ductile in nature [40-42]. Our finding of lower B/G and σ compared to their critical values indicates that superhard material is brittle at room temperature. It is well known that for stable and elastic material, the value of σ should be less than 0.26. The values of 'σ' evaluated for BC_2N superhard materials are smaller than their critical value. It indicates that BC_2N superhard materials are stable against shear. The stronger degree of covalent bonding leads to higher hardness. The compressibility, hardness, ductility, toughness, brittleness, and bonding characteristic of the material are too well connected with the second-order elastic constants.

3.2. *Ultrasonic Velocity and allied parameters*

In the present analysis, we have correlated the mechanical and isotropic behavior of the superhard material with the ultrasonic velocity. We have calculated the longitudinal ultrasonic velocity (V_L), ultrasonic shear velocity (V_S), the Debye average velocity (V_D), and the thermal relaxation time (τ) for BC_2N superhard material. The data for the temperature-dependent density (ρ) and thermal conductivity (k) of BC_2N superhard material presented in Table 3 and have been taken from the literature [37]. The values of temperature-dependent thermal energy density (E_0) and specific heat per unit volume (C_V) were calculated using the Tables of physical constant and Debye temperatures and acoustic coupling constants (D_L and D_S) are presented in Table 3.

Table 3. Density (ρ: × 10^3 kg m^{-3}), specific heat per unit volume (C_V: × 10^5Jm^{-3}K^{-1}), thermal energy density (E_0: × 10^7Jm^{-3}), thermal conductivity (k: × 10^2 Wm^{-1}K^{-1}), and acoustic coupling constant (D_L, D_S) of BC_2N superhard material.

Temp	ρ	E_0	C_V	k	D_L	D_S
200	3.44	2.25	3.92	58.45	48.112	1.924
300	3.42	8.2	7.94	24.40	48.936	1.924
400	3.40	17.74	10.95	15.00	49.553	1.924
500	3.38	29.90	12.94	11.50	49.987	1.924
600	3.36	43.99	14.07	9.05	50.335	1.924
700	3.34	58.99	15.00	9.687	50.533	1.924
800	3.32	74.59	15.85	7.20	50.646	1.924
900	3.30	91.59	16.44	6.30	50.766	1.924
1000	3.28	108.52	16.78	5.80	50.865	1.924

It is clear from Table 3 that for all temperatures, the values of D_L are larger than D_S for BC_2N superhard material. It indicates that the transformation of ultrasonic energy into thermal energy for the ultrasonic shear wave is less than that for the longitudinal ultrasonic waves.

The angular dependences of ultrasonic wave velocity (V_L, V_{S1}, $V_{S2,}$ and V_D) at different temperatures are shown in Figs. 1-4 with the z-axis of the crystal. Figs. 1 and 2 show that velocities V_L and V_{S1} of BC_2N superhard material have minima and maxima at 45° respectively with the z-axis of the crystal while V_{S2} increases with the angle from the z-axis (Fig. 3). The anomalous behavior of angle-dependent velocity is due to the combined effect of SOECs and density. The properties of the angle-dependent velocity curves in the present work are similar to the nature of angle-dependent velocity curves found for other hexagonal types of material [43,44]. Thus, the angle dependence of the velocities in BC_2N superhard material is justified.

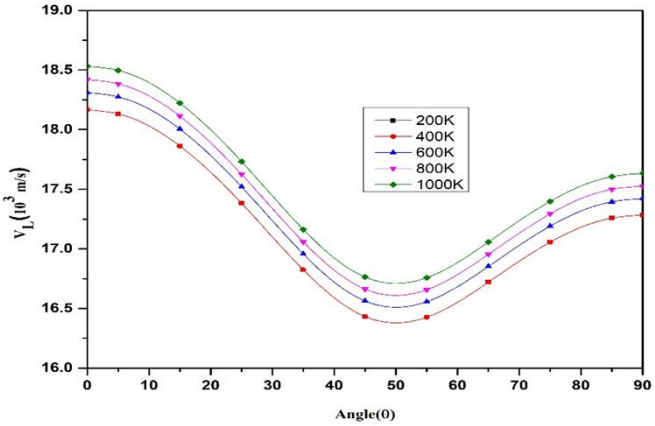

Fig. 1. V_L vs. angle with the z-axis of crystal.

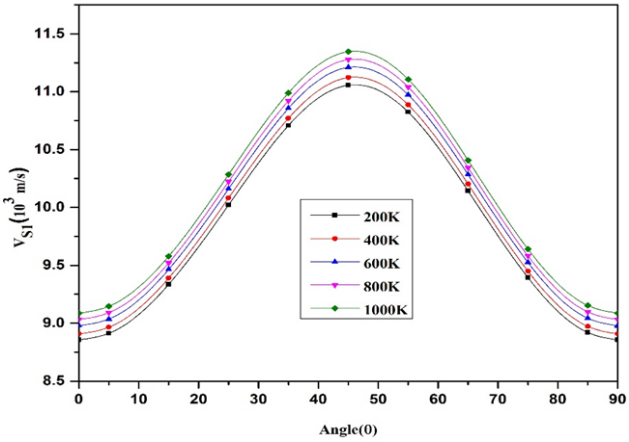

Fig. 2. V_{S1} vs. angle with the z-axis of crystal.

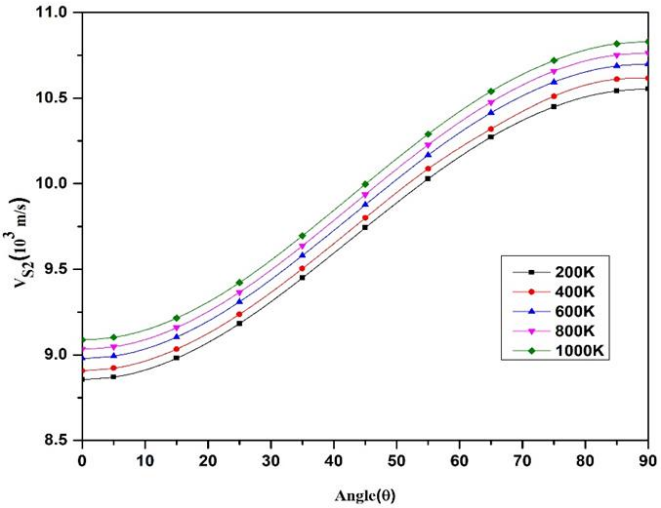

Fig. 3. V_{S2} vs. angle with the z-axis of crystal.

Fig. 4 shows the variation of the Debye average velocity (V_D) with the angle made with the z-axis of the crystal. It is clear that V_D increases with the angle and reaches a maximum of 55° for BC_2N superhard materials. Since V_D is calculated using the velocities V_L, $V_{S1,}$ and V_{S2} [45,46], VD's angle variation is influenced by the constituent ultrasonic velocities. The maximum value of V_D at 55° is due to a significant decrease in longitudinal wave velocities and an increase in shear wave velocities. The average sound wave velocity may be determined to be maximum when a sound wave travels at 55° angles with the z-axis of these crystals.

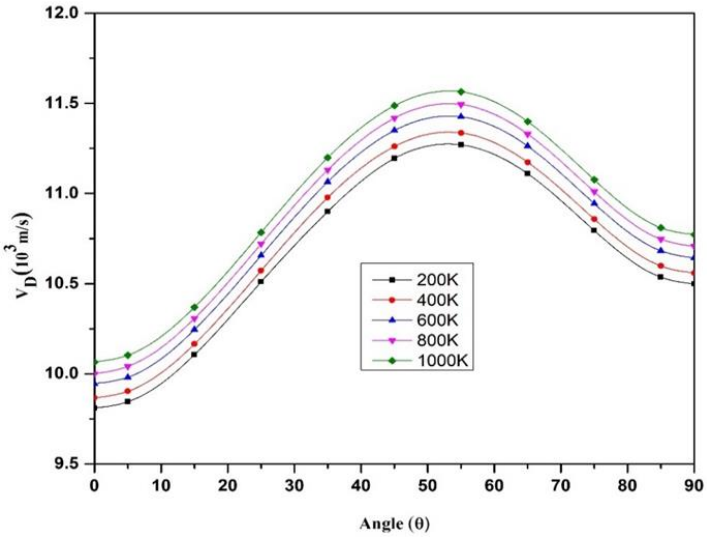

Fig. 4. V_D vs. angle with the unique axis of the crystal.

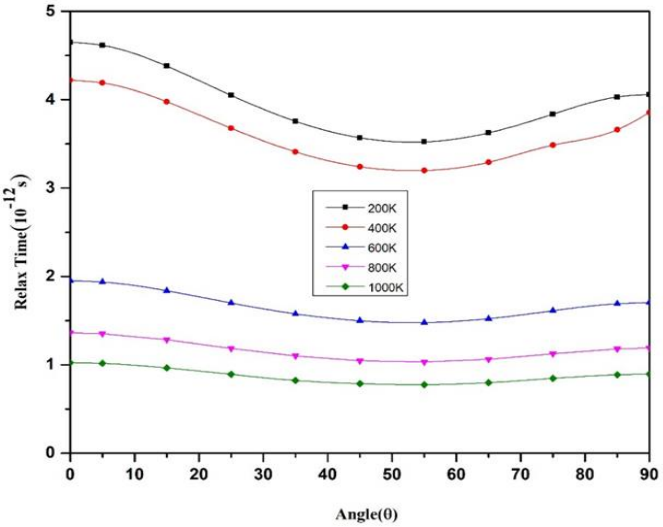

Fig. 5. Relaxation time vs. angle with the z-axis of crystal.

The calculated thermal relaxation time 'τ' is visualized in Fig. 5. The angle-dependent thermal relaxation time curves track the reciprocal nature of V_D as $\tau \propto 3k/C_V V_D^2$. Thermal relaxation time for BC_2N superhard material is mainly affected by thermal conductivity. The thermal relaxation time 'τ' is of order at picoseconds for hexagonally structured materials [43,47]. Therefore, the evaluated thermal relaxation time explains the hexagonal structure of superhard material. The minimum 'τ' for wave propagation along $\theta = 55^0$ implies that the re-establishment time for the equilibrium distribution of thermal phonons will be minimum for wave propagation along this direction.

3.3. *Ultrasonic attenuation due to phonon-phonon interaction and thermal relaxation phenomena*

In evaluating ultrasonic attenuation, it is supposed that the wave is propagating along the unique axis [<001> direction] of BC_2N superhard material. The ultrasonic attenuation coefficient divided by frequency squared $(A/f^2)_{Akh}$ is calculated for the longitudinal wave $(A/f^2)_L$ and the shear wave $(A/f^2)_S$ using Eq. 12 under the condition $\omega\tau<<1$ at different temperatures. Eq. 13 has been used to calculate the thermo-elastic loss divided by frequency square $(A/f^2)_{Th}$. The values of temperature-dependent $(A/f^2)_L$, $(A/f^2)_S$, $(A/f^2)_{Th,}$ and total attenuation $(A/f^2)_{total}$ of BC_2N superhard material are presented in Figs. 6-7.

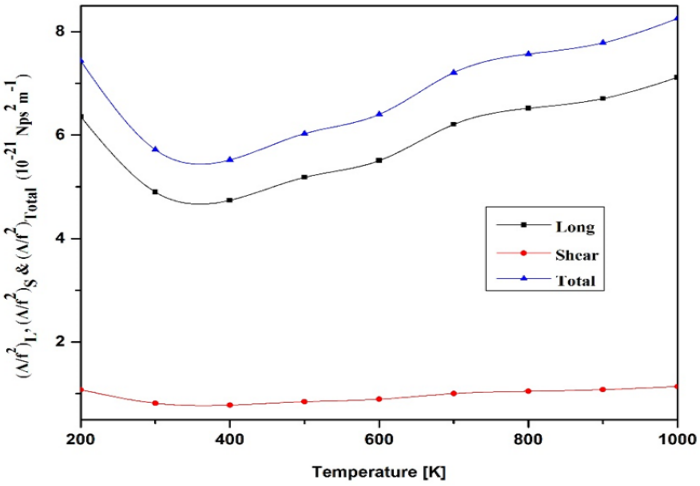

Fig. 6. Long and shear attenuation vs. temperature of BC_2N material.

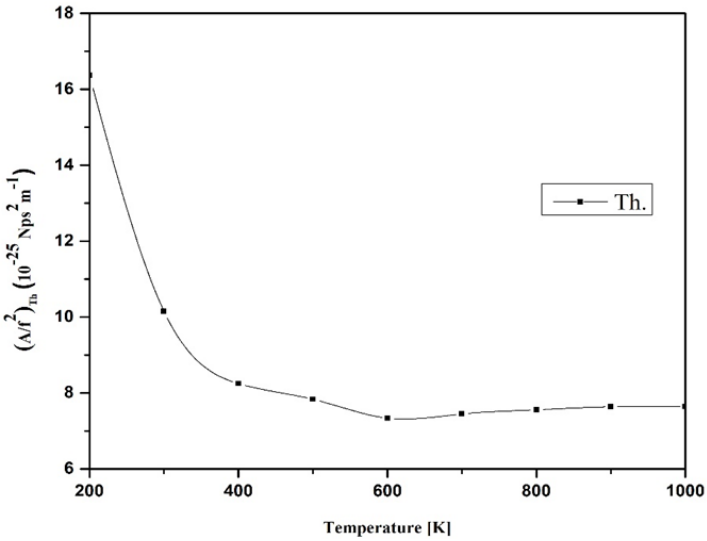

Fig. 7. Th. attenuation vs. temperature of BC_2N high entropy alloy.

In the present investigation, the ultrasonic wave propagates along the z-axis of the crystal; the Akhieser type of loss of energy for longitudinal and shear wave increases with the temperature and minimum at temperature 400 K of the superhard material (Fig. 6). $(A/f^2)_{Akh}$ is proportional to D, E_0, τ, and V^3 (Eqs. 12 and 14). Table 3 shows that' E_0' and 'V' are increasing with temperature. Hence Akhieser losses in BC_2N superhard material are overwhelmingly affected by E_0 and the 'k'.

Therefore, the ultrasonic attenuation increases due to the reduction in the thermal conductivity. Thus, ultrasonic attenuation is mainly governed by the phonon-phonon interaction mechanism. A comparison of the UA could not be made due to the lack of experimental data in the literature.

Fig. 7 indicates that the thermo-elastic loss is very small compared to Akhieser loss, and ultrasonic attenuation for longitudinal wave $(A/f^2)_L$ is greater than that of shear wave $(A/f^2)_S$. This reveals that ultrasonic attenuation due to phonon-phonon interaction along longitudinal wave is governing factor for total attenuation $((A/f^2)_{Total} = (A/f^2)_{Th} + (A/f^2)_L + (A/f^2)_S)$. The total attenuation is mainly affected by thermal energy density and thermal conductivity. Thus, it may predict that at temperature (400K), the BC_2N superhard material behaves as its purest form and is more ductile as evinced by minimum attenuation, while at other temperatures, BC_2N superhard material is least ductile. Therefore, at temperature 400 K, there will be the least impurity in BC_2N superhard material. The minimum UA for BC_2N superhard material minimum defends its relatively stable hexagonal type structure state.

4. Conclusion

Based on the above conversation, it is valuable to state that:

- The theory using a simple interaction potential model for evaluating temperature-dependent higher-order elastic constants and ultrasonic attenuation is validated for the hexagonally BC_2N superhard material.
- Elastic properties of BC_2N superhard material imply that this superhard compound is mechanically stable.
- The order of thermal relaxation time for BC_2N superhard material is found in picoseconds, which justifies their HCP structure. As 'τ' has the smallest value along $\theta = 55°$, at all temperatures, the time for re-establishment of the equilibrium distribution of phonons will be minimum for the wave propagation in this direction.
- Due to the phonon-phonon interaction mechanism, ultrasonic attenuation is predominant over total attenuation as a governing factor of thermal conductivity and thermal energy density.
- The mechanical properties of the BC_2N superhard material are better than at temperature 400 K to other temperatures.
- BC_2N superhard material behaves in its purest form at 400 K temperature and is more ductile, demonstrated by the minimum attenuation, while at other temperatures, these are least ductile.

The study can be beneficial for the processing and non-destructive characterization of superhard materials. These results will provide a ground for investigating the major thermophysical properties in the field of other superhard compounds.

Acknowledgment

One of authors (S. Rai) is thankful to Council for Scientific and Industrial Research - University Grant Commission (CSIR - UGC) for providing financial assistance in form of CSIR - Junior Research Fellowship (1500/CSIR-UGC NET dec, 2017) India.

References

1. J. L. He, Z. Liu, D. L. Yu, B. Xu, and Y. J. Tian, Front. Phys. China **2**, 186 (2007). https://doi.org/10.1007/s11467-007-0031-6
2. X. D. Bai, E.G. Wang, and J. Yu, Appl. Phys. Lett. **77**, 67 (2000). https://doi.org/10.1063/1.126879
3. Y. Chen, J. C. Barnard, R.E. Palmer, M.O. Watanable, and T. Sasaki, Phys. Rev. Lett. **83**, 2406 (1999). https://doi.org/10.1103/PhysRevLett.83.2406
4. T. Nakajima and M. Koh, Carbon **35**, 203 (1997). https://doi.org/10.1016/S0008-6223(96)00143-1
5. V. L. Solozhenko, D. Andrault, G. Fiquet, M. Mezouar, and D.C. Rubie, Appl. Phys. Lett. **78**, 1385 (2001). https://doi.org/10.1063/1.1337623
6. Z. X. Cao, M. L. Lio, and T. E. Oechsner, J. Vac. Sci.Technol. B: Microelectronics Nanometer Struct. Process., Measurement Phenomena **20**, 2275 (2002). https://doi.org/10.1116/1.1518973
7. D. M. Teter, MRS Bull. **23**, 22 (1998). https://doi.org/10.1557/S0883769400031420
8. D. Onn, A. Witek, Y. Qiu, T. Anthony, and W. Banholzer, Phy. Rev. Lett. **68**, 2806 (1992). https://doi.org/10.1103/PhysRevLett.68.2806
9. J. Olson, R. Pohl, J. Vandersande, A. Zoltan, T. Anthony, and W. Banholzer, Phys. Rev. B. **47**, 14850 (1993). https://doi.org/10.1103/PhysRevB.47.14850
10. L. Wei, P. Kuo, R. Thomas, T. Anthony, and W. Banholzer, Phys. Rev. Lett. **70**, 3764 (1993). https://doi.org/10.1103/PhysRevLett.70.3764
11. Y. Zhao, D. He, L. Daemen, T. Shen, R. Schwarz, Y. Zhu, D. Bish, J. Huang, J. Zhang, and G. Shen, J. Mater. Res. **17**, 3139 (2002). https://doi.org/10.1557/JMR.2002.0454
12. V. L. Solozhenko, D. Andrault, G. Fiquet, M. Mezouar, and D. C. Rubie, Appl. Phys. Lett. **78**, 1385 (2001). https://doi.org/10.1063/1.1337623
13. A. R. Badzian, Mater. Res. Bull. **16**, 1385 (1981). https://doi.org/10.1016/0025-5408(81)90057-X
14. S. Nakano, M. Akaishi, T. Sasaki, and S. Yamaoka, Chem. Mater. **6**, 2246 (1994). https://doi.org/10.1021/cm00048a011
15. S. N. Sadeghi, S. M. V. Allaei, M. Zebarjadi, and K. Esfarjani, J. Mater. Chem. C **8**, 15705 (2020). https://doi.org/10.1039/D0TC01615B
16. P. Chakraborty, G. Xiong, L. Cao, and Y. Wang, Carbon **139**, 85 (2018). https://doi.org/10.1016/j.carbon.2018.06.025
17. B. H. Yu, C. L. Wang, X. Y. Song, Q. J. Sun, and D. Chen, J. Appl. Phys. **123**, 135103 (2018). https://doi.org/10.1063/1.5022517
18. J. Boland, Nature **510**, 220 (2014). https://doi.org/10.1038/510220a
19. C. H. Li, H. Y. Zhao, H. L. Ma, Y. L. Hou, Y. B. Zhang, M. Yang, and X. W. Zhang, J. Adv. Manufac. Technol. **81**, 2027 (2015). https://doi.org/10.1007/s00170-017-1159-3
20. C. Linsmeier and M. Reinelt, Adv. Mater. **59**, 120 (2009). https://doi.org/10.4028/www.scientific.net/AMR.59.120
21. X. B. Liu, Y. Y. Ch, S. N. Tkachev, C. B. Bina, and S. D. Jacobsen, Sci. Rep. **7**, 42917 (2017). https://doi.org/10.1038/srep42921
22. J. L. He, Z. Y. Liu, D. Yu, D. Xu, and Y. J. Tian, Chem. Phys. Lett. **340**, 42 (2001). https://doi.org/10.1007/s11467-007-0031-6
23. J. Yu, E.G. Wang, J. Ahn, S. F. Yoon, Q. Zhang, J. Cui, and M. B. Turbostratic, J. Appl. Phys. **87**, 4022 (2000). https://doi.org/10.1063/1.372456

24. Z. X. Cao, L.M. Liu, and H. Oechsner, J. Vacu. Sci. Technol. B. **20**, 2275 (2002). https://doi.org/10.1116/1.1518973
25. P. K. Yadawa, Pramana-Ind. J. Phys. **76**, 613 (2011). http://dx.doi.org/10.1007/s12043-011-0066-7
26. D. K. Pandey, P. K. Yadawa, and R. R. Yadav, Mater. Lett. **61**, 5194 (2007). https://doi.org/10.1016/j.matlet.2007.04.028
27. W. Voigt, Lehrbuch der kristallphysik (mitausschluss der kristalloptik) (Leipzig Berlin, B.G. Teubner, 1928). https://www.springer.com/gp/book/9783663153160
28. A. Reuss, ZAMM - J. Appl. Math. Mech./Zeitschrift für Angewandte Mathematik und Mechanik. **9**, 49 (1929). https://doi.org/10.1002/zamm.19290090104
29. R. Hill, Proc. Phys. Soc. A **65**, 349 (1952). https://doi.org/10.1088/0370-1298/65/5/307
30. N. Turkdal, E. Deligoz, H. Ozisik, and H. B. Ozisik, Ph. Transit. **90**, 598 (2017). https://doi.org/10.1080/01411594.2016.1252979
31. P. F. Weck, E. Kim, V. Tikare, and J. A. Mitchell, Dalton Trans. **44**, 18769 (2015). https://doi.org/10.1039/C5DT03403E
32. D. Singh, D. K. Pandey, P. K. Yadawa, and A. K. Yadav, Cryogen. **49**, 12 (2009). https://doi.org/10.1016/j.cryogenics.2008.08.008
33. V. V. Manju, S. Divakara, and R. Somashekar, J. Sci. Res. **12**(4), 607 (2020). https://doi.org/10.3329/jsr.v12i4.47269
34. R. R. Koireng P.C. Agarwal, and A. Gokhroo, J. Sci. Res. **13**(1), 21 (2021). https://doi.org/10.3329/jsr.v13i1.47327
35. S. P. Singh, P. K. Yadawa, P. K. Dhawan, A. K. Verma, and R. R. Yadav, Cryogenics **100**, 105 (2019). https://doi.org/10.1016/j.cryogenics.2019.03.006
36. D. Singh, P. K. Yadawa, and S. K. Sahu, Cryogenics **50**, 476 (2010). https://doi.org/10.1016/j.cryogenics.2010.04.005
37. S. N. Sadeghi, S. M. V. Allaei, M. Zebarjadi, and K. Esfarjani, J. Mater. Chem. C **8**, 15705 (2020). https://doi.org/10.1039/D0TC01615B
38. P. K. Yadawa, Arabian J. Sci. Eng. **37**, 255 (2012). https://doi.org/10.1007/s13369-011-0153-6
39. P. K. Yadawa, Adv. Mat. Lett. **2**, 157 (2011). https://doi.org/10.5185/amlett.2010.12190
40. N. Yadav, S. P. Singh, A. K. Maddheshiya, P. K. Yadawa, and R. R. Yadav, Phase Transitions. **93**, 883 (2020). https://doi.org/10.1080/01411594.2020.1813290
41. L. Liu, Z. Zhao, T. Yu, S. Zhang, J. Lin, and G. Yang, J. Phys. Chem. C **122**, 6801 (2018). https://doi.org/10.1021/acs.jpcc.9b05446
42. S. N. Sadeghi, S. M. V. Allaei, M. Zebarjadi, and K. Esfarjani, J. Mater. Chem. C **8**, 15705 (2020). https://doi.org/10.1039/D0TC01615B
43. P. K. Yadawa, IOP Conf. Series: Mater. Sci. Eng. **42**, ID 012034 (2012). https://doi.org/10.12691/jmpc-3-1-1
44. P. K. Yadawa, Ceramics-Silikaty. **55**, 127 (2011). https://doi.org/10.12691/jmpc-3-1-1
45. A. K. Jaiswal, P. K. Yadawa, and R. R. Yadav, Ultrasonics **89**, 22 (2018). https://doi.org/10.1016/j.ultras.2018.04.009
46. S. P. Singh, G. Singh, A. K. Verma, P. K. Yadawa, and R. R. Yadav, Pramana-J. Phys. **93**, 83 (2019). https://doi.org/10.1007/s12043-019-1846-8
47. D. K. Pandey, P. K. Yadawa, and R. R. Yadav, Mater. Lett. **61**, 4747 (2007). https://doi.org/10.1016/j.matlet.2007.03.031